Check for updates

Special Collection

Observation of Interfacial Degradation of Li_6PS_5Cl against Lithium Metal and $LiCoO_2$ via *In Situ* Electrochemical Raman Microscopy

Yundong Zhou,[a, b, c] Christopher Doerrer,[c, d] Jitti Kasemchainan,[c, d] Peter G. Bruce,[c, d] Mauro Pasta,[c, d] and Laurence J. Hardwick*[a, b, c]

Sulfide-based Li^+ conducting solid electrolytes, such as argyrodite, Li_6PS_5Cl, for all-solid-state batteries can have comparable ionic conductivities with liquid electrolytes. However, the interface between sulfide containing solid electrolytes and Li metal and Li-ion positive electrodes has been found to be unstable, leading to poor cell performance and cycling. Understanding the *in situ* evolution of interfacial layers between the electrolyte and both electrodes is of paramount importance for designing stable and long-life solid-state batteries. Here, *in situ* Raman microscopy was used to study the interface between Li_6PS_5Cl electrolyte and metallic Li and $LiCoO_2$. Under potential control, Raman microscopy identified the appearance of degradation products (Li_2S, P_2S_x and polysulfides) at the electrode/solid electrolyte interface.

1. Introduction

All-solid-state lithium-ion batteries (ASSB), utilizing non-flammable ceramic solid-state electrolytes, are attracting intensive interest due to perceived greater safety over Li-ion batteries containing organic liquid electrolytes.[1] Recent research efforts have been driven by sulfide family of solid-state electrolytes that display comparable room temperature Li^+ ionic conductivities to liquid electrolytes, for example, $Li_{10}GeP_2S_{12}$ (1.2×10^{-2} S cm^{-1})[2] and Li_6PS_5Cl (in the range of 10^{-3}–10^{-2} S cm^{-1}).[3] However, the cycle-life performance of ASSB reported with sulfide based solid electrolytes are typically limited to less than 100 cycles before substantial capacity fade.[4] This is due in part because sulfide solid electrolytes possess a narrow electrochemical stability window.[5] Out of the sulphide group of electrolytes, the argyrodite Li_6PS_5Cl, is attracting particular attention because of its aforementioned high conductivity and good processability. However, it shows interfacial instability towards electrode active materials.[6] As a result, the discharge capacities of the cells prepared with Li_6PS_5Cl electrolyte rapidly decreased to below 100 mAh g^{-1} with $LiCoO_2$, below 50 mAh g^{-1} with $LiMn_2O_4$ and $LiNi_{1/3}Mn_{1/3}Co_{1/3}O_2$ after only 25 cycles. The oxidation products of Li_6PS_5Cl at the interface with these positive electrode materials have been resolved by XPS (X-ray photoelectron spectroscopy) and were found to be S, P_2S_x ($x\geq5$), phosphates, LiCl, lithium polysulfides, which were ionically insulating and caused the rapid capacity decay.[6]

The interfacial instability between the solid electrolytes and electrodes is one of the limiting factors for the utilisation of ASSB's.[7] Application of pressure of ca. 7 MPa upon solid-state cells was further identified to be critical for their performance, as the pressure strongly influences the Li creep behaviour during stripping.[8] When the potential of the negative or positive electrode is outside of the electrochemical stability window of the solid electrolyte, the solid electrolyte will decompose and form an interfacial layer. A comprehensive first-principle study revealed[5] most solid electrolyte materials have a limited electrochemical window and can be easily degraded in contact with common cathode materials. Thus, the characterisation and understanding of the interface between solid electrolytes and electrodes are very important.

The buried nature of these interfaces presents certain challenges in order to characterise them with traditional surface characterisation techniques, whether *ex situ*, *in situ* or operando. Predominantly, *ex situ* characterisation of solid electrolyte/Li metal and solid electrolyte/cathode interfaces have been undertaken. The interface between $Li_7La_3Zr_2O_{12}$ and $LiCoO_2$ was studied after being annealed at different temperatures.[7b] Breakdown products such as $La_2Zr_2O_7$, Li_2CO_3 and $LaCoO_3$ were

[a] Dr. Y. Zhou, Prof. L. J. Hardwick
Stephenson Institute for Renewable Energy
University of Liverpool,
Chadwick Building, Peach Street,
Liverpool L69 7ZF, UK
E-mail: hardwick@liverpool.ac.uk
[b] Dr. Y. Zhou, Prof. L. J. Hardwick
Department of Chemistry
University of Liverpool,
Crown St, Liverpool L69 7ZD, UK
[c] Dr. Y. Zhou, C. Doerrer, Dr. J. Kasemchainan, Prof. P. G. Bruce, Prof. M. Pasta, Prof. L. J. Hardwick
The Faraday Institution,
Quad One, Becquerel Avenue
Harwell Campus, Didcot OX11 0RA, UK
[d] C. Doerrer, Dr. J. Kasemchainan, Prof. P. G. Bruce, Prof. M. Pasta
Department of Materials
Parks Road
University of Oxford,
Oxford OX1 3PH, UK

Supporting information for this article is available on the WWW under https://doi.org/10.1002/batt.201900218

Special Collection *An invited contribution to a Special Collection on Electrolytes for Electrochemical Energy Storage*

© 2020 The Authors. Published by Wiley-VCH Verlag GmbH & Co. KGaA. This is an open access article under the terms of the Creative Commons Attribution License, which permits use, distribution and reproduction in any medium, provided the original work is properly cited.

© 2020 The Authors. Published by Wiley-VCH Verlag GmbH & Co. KGaA

identified with a combination of synchrotron XRD (X-ray diffraction), XAS (X-ray absorption spectroscopy), and XPS techniques. Co and La were also found to diffuse across the interface. $Li_7La_3Zr_2O_{12}$ was also found to be unstable with $LiNi_{0.33}Mn_{0.33}Co_{0.33}O_2$ with the formation of $La_2Zr_2O_7$ and $LaNiO_3$.[9] The interfacial resistance at the $Li_{10}GeP_2S_{12}/LiCoO_2$ interface was found to increase with cycling.[10] In another study, the degraded $Li_{10}GeP_2S_{12}/LiCoO_2$/Indium solid-state cells were disassembled, and the composite cathode was characterised with XPS.[11] It was revealed that $Li_{10}GeP_2S_{12}$ was oxidised with the formation of S and $Li_2P_2S_6$ at the interface. This, together with the formation of Li-depletion zone on the $Li_{10}GeP_2S_{12}$ at the interface caused the high interfacial resistance and capacity degradation. As previously mentioned, the interface between argyrodite solid electrolytes Li_6PS_5Cl and $LiCoO_2$, $LiNi_{0.33}Mn_{0.33}Co_{0.33}O_2$, and $LiMn_2O_4$ cathodes were studied by *ex situ* XPS.[6] The degradation products included S, Li_2S_n, P_2S_x, phosphates and LiCl at the interface between the argyrodite and cathodes after cell cycling. Li_6PS_5X (X=Cl, Br, I) were also found to decompose into Li_3P, Li_2S and LiX with metallic Li deposition by *in situ* XPS.[12] This result was consistent with molecular dynamic studies.[13] Besides the *in situ* study of the structure of some materials by *in situ* XRD[14] and neutron diffraction technique,[15] there are only a handful of *in situ* studies on the solid electrolyte/electrode interface, such as the *in situ* scanning transmission electron microscopy (STEM) coupled with electron energy loss spectroscopy (EELS) study of the interface between $LiCoO_2$ and lithium phosphorus oxynitride (LiPON)[16] and visualisation of the electric potential distribution at the interface of $LiCoO_2$ and $Li_{1-x-y}Al_yTi_{2-y}Si_xP_{3-x}O_{12}$ using electron holography technique.[17]

The ability to do *in situ* observation of the solid electrolyte/electrode interface is paramount for understanding the performance and design interfacial strategies for all solid-state batteries. Raman microscopy is a powerful technique for the detection of structural and chemical information and has been used extensively for studying battery materials.[18] However, *in situ* Raman microscopy has not so far being fully explored in the study of solid electrolyte/electrode interface due to challenges of optically accessing solid-solid interfaces. In this study, *in situ* Raman microscopy was implemented to study the interfacial evolution during cycling of Li_6PS_5Cl electrolytes with Li metal and $LiCoO_2$.

2. Results and Discussion

The Raman spectrum of pristine Li_6PS_5Cl is shown in Figure 1. Peaks at 199, 272, 425, 573, and 600 cm^{-1} are all attributed to vibrational modes of PS_4^{3-} within Li_6PS_5Cl, as shown in Table 1 and corresponds with previously reported spectra.[19] The peak fitting results including the peak centre frequencies (cm^{-1}) and full width at half maximum (FWHM, cm^{-1}) are presented in Table S1. The XRD spectra of the powder in Figure S1 shows the composition is Li_6PS_5Cl phase, with a minor Li_2S impurity. Raman measurements did not detect any Li_2S on the pristine Li_6PS_5Cl powder sample. The ionic conductivity of the Li_6PS_5Cl after ball-milling was found to be 1.1×10^{-3} S cm^{-1}, with the impedance spectra and fitting shown in Figure S2.

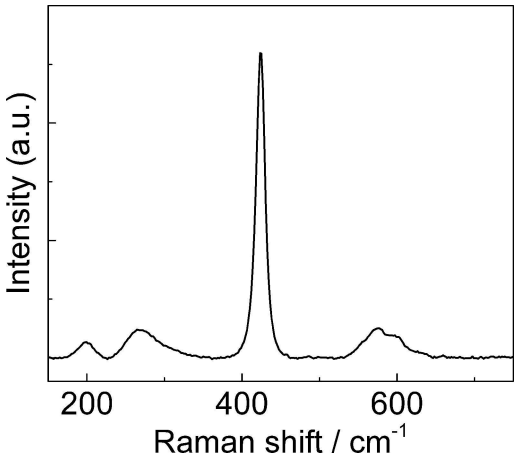

Figure 1. Raman spectrum of Li_6PS_5Cl.

Table 1. Peak assignments for the pristine Li_6PS_5Cl.

Frequency [cm^{-1}]	Assignment	Ref
199	PS_4^{3-}	[19]
272	δ_{def}(S–P–S) in PS_4^{3-}	[20]
425	$\upsilon_s(PS_4^{3-})$ in PS_4^{3-}	[20]
573	PS_4^{3-}	[19]
600		

Cyclic voltammetry measurements of the solid-state electrolyte Li_6PS_5Cl from −0.5 to 7 V vs Li^+/Li (1st cycle) and 8 V vs Li^+/Li (2nd cycle) at 30 °C is shown in Figure S3. This result is consistent with the 7 V vs Li^+/Li stability of Li_6PS_5Cl previously reported.[21] The Li_6PS_5Cl demonstrated stable Li plating and stripping from −0.5 up to 8 V vs Li^+/Li, although the inset shows instabilities are observed, via current peaks from 2 V vs Li^+/Li, highlighting the limited electrochemical stability window of this material.

To observe the Li_6PS_5Cl interface with metallic Li under potential control, a Li/ Li_6PS_5Cl/ Cu cell was assembled within an *in situ* Raman cell and a negative potential was applied between Cu vs. Li. Initially, a constant −0.1 V vs Li was applied at the positive Cu electrode to get continuous Li deposition. The current upon application of the potential was shown in Figure S4. As shown in Figure 2(a), after holding the potential for 2 hours, two new peaks at 383 and 470 cm^{-1} appear, in addition to the peaks from Li_6PS_5Cl. The peak at 383 cm^{-1} can be assigned as $\upsilon_{Li\text{-}S}$,[20] from Li_2S as Li deposition takes place. The peak at 470 cm^{-1} can be assigned to the S–S stretching mode of S_2 ions in CuS.[22] The formation of CuS likely occurs from the reaction of the Cu current collector with phosphorous sulphides ($P_xS_y^{n-}$). The peak assignments are shown in Table 2. In Figure 2(b), a matching cell was applied with a potential of −0.1 V vs Li for 1 hour and −0.2 V vs Li for 1 hour. Again, the same new bands at 383 and 470 cm^{-1} also appeared. The potential was then reversed to positive 0.1 V and up to 0.4 V vs Li^+/Li. The newly formed peaks remained present, highlighting that the CuS and Li_2S are not removed at these potentials and

© 2020 The Authors. Published by Wiley-VCH Verlag GmbH & Co. KGaA

25666223, 2020, 7, Downloaded from https://chemistry-europe.onlinelibrary.wiley.com/doi/10.1002/batt.201900218 by University of Ulsan, Wiley Online Library on [11/11/2025]. See the Terms and Conditions (https://onlinelibrary.wiley.com/terms-and-conditions) on Wiley Online Library for rules of use; OA articles are governed by the applicable Creative Commons License

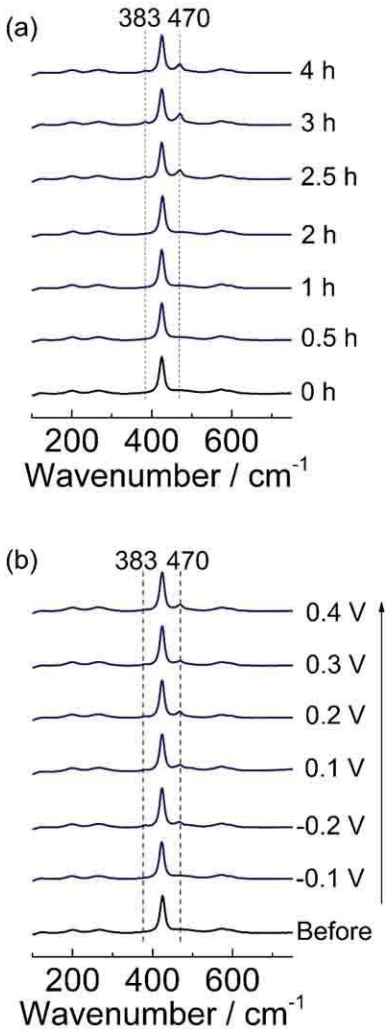

Figure 2. *In situ* Raman spectra of Li_6PS_5Cl/Li interface in Li / Li_6PS_5Cl / Cu cell under a) constant potential of −0.1 V vs. Li^+/Li; b) under variable potential.

once formed, remain at the Li/Cu electrode interface. The reduction of Li_6PS_5Cl by metallic Li into Li_2S is consistent with previous reports by XPS results[12] and molecular dynamic simulations.[13] The fitted Raman peaks (Table S2) generally show minor variation in terms of peak position with respect to time or potential, apart from the δ_{def} (S–P–S) vibration that is seen to red-shift by ca. 5 cm^{-1} from initially position for 272 cm^{-1} immediately after potential is applied .The other main Li_6PS_5Cl bands do not shift their position, however once potential is applied vibrations associated with PS_4^{3-} line shapes broaden significantly, by almost doubling their FWHM. This could be associated with initial decomposition of Li_6PS_5Cl once contacted with lithium as the material becomes more amorphous.

The stability of Li_6PS_5Cl with $LiCoO_2$ was studied with the *in situ* Raman cell during delithiation and lithiation, as shown in Figure 3. The cell exhibited first cycle charge and discharge capacities of 173 and 130 mAh g^{-1} respectively. The capacities obtained in the Raman cell mirror those found generally in the literature, thereby demonstrating that representative electrochemical performance can be achieved within the Raman cell. The *in situ* Raman measurements are shown in Figure 4. In Figure 4(a), at open circuit potential, 2.38 V, the peak of PS_4^{3-} from Li_6PS_5Cl at 421 cm^{-1}[20] and E_g and A_{1g} of $LiCoO_2$ at 484 and 593 cm^{-1},[23] can be observed respectively. When the cell was charged to 3.97 V, the E_g and A_{1g} peaks decreased in intensity. This is associated with an increase in electronic conductivity from initial Li de-intercalation that reduces the optical skin depth of Li_xCoO_2 and has been reported in previous investigations of $LiCoO_2$ using *in situ* Raman microscopy.[23] At 3.98 V, the E_g and A_{1g} peaks disappear into the background noise, while new peaks appeared at 151, 219 and 473 cm^{-1} from S,[24] and at 378 and 705 cm^{-1} from P_2S_x ($x = 5$ or 6 or 7).[25] These new peaks remain up to 4.2 V. During discharge in Figure 4(b), the peaks from S and P_2S_x remained present down to a potential of 2.5 V. The E_g and A_{1g} bands of $LiCoO_2$ reappeared from 3.57 V. The formation of S and P_2S_x at the interface of Li_6PS_5Cl and $LiCoO_2$ are consistent with previously reported XPS results.[6] The majority of fitted peaks from *in situ* Raman spectra (Table S3) showed small variation in terms of peak position/cm^{-1} and full width at half maximum (FWHM/cm^{-1}) that were within experimental error. However, there was peak broadening observed of the most intense band of Li_6PS_5Cl at ca. 422 cm^{-1} from a FWHM of ca. 20 cm^{-1} at 2.8 V to ca. 40 cm^{-1} at potentials above 3.9 V. The broadening is reversible as when the potential is lowered below 3.5 V the peak shape narrow returns to FWHM of ca. 20 cm^{-1}.

Table 2. Peak assignments for the Li_6PS_5Cl interface with Li deposition (Figure 2) and $LiCoO_2$ under potential control (Figure 4).

Frequency [cm^{-1}]	Assignment	Compound	Ref
151	S–S–S bending	S_8	[24, 26]
219	S–S–S bending	S_8	[24, 26]
272	δ_{def}(S–P–S) in PS_4^{3-}	Li_6PS_5Cl	[20]
378	mixed symmetric P–P and P–S stretching modes (A_{1g})	P_2S_x (x = 5 or 6 or 7)	[24b, 25a, 25b, 25e, 25 g]
383	T_{2g} phonon mode in Li_2S	Li_2S	[27]
421–425	$\upsilon_s(PS_4^{3-})$ in PS_4^{3-}	Li_6PS_5Cl	[20]
470	S–S stretching mode of S_2^{2-}	CuS	[28]
473	S–S bending	S_8	[24, 26]
484	O–Co–O bending (E_g)	$LiCoO_2$	[23, 29]
593	O–Co–O stretch (A_{1g})	$LiCoO_2$	[23, 29]
573	PS_4^{3-}	Li_6PS_5Cl	[19]
600	PS_4^{3-}	Li_6PS_5Cl	[19]
705	P–S stretching vibration of terminal S	P_2S_x (x = 5 or 6 or 7)	[24b, 25a, 25b, 25e, 25 g]

© 2020 The Authors. Published by Wiley-VCH Verlag GmbH & Co. KGaA

25666223, 2020, 7, Downloaded from https://chemistry-europe.onlinelibrary.wiley.com/doi/10.1002/batt.201900218 by University of Ulsan, Wiley Online Library on [11/11/2025]. See the Terms and Conditions (https://onlinelibrary.wiley.com/terms-and-conditions) on Wiley Online Library for rules of use; OA articles are governed by the applicable Creative Commons License

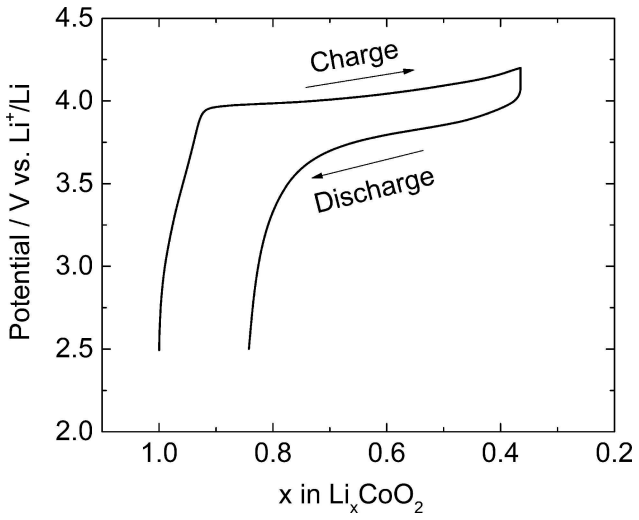

Figure 3. Charge and discharge profile for $LiCoO_2/Li_6PS_5Cl/Li$ all solid-state cell measured within the in situ Raman cell. During charging, 0.63Li was removed from Li_xCoO_2, and 0.48Li was reinserted during discharging, which corresponds to ca. 173 and 130 mAh g^{-1} first cycle charge and discharge capacities, respectively.

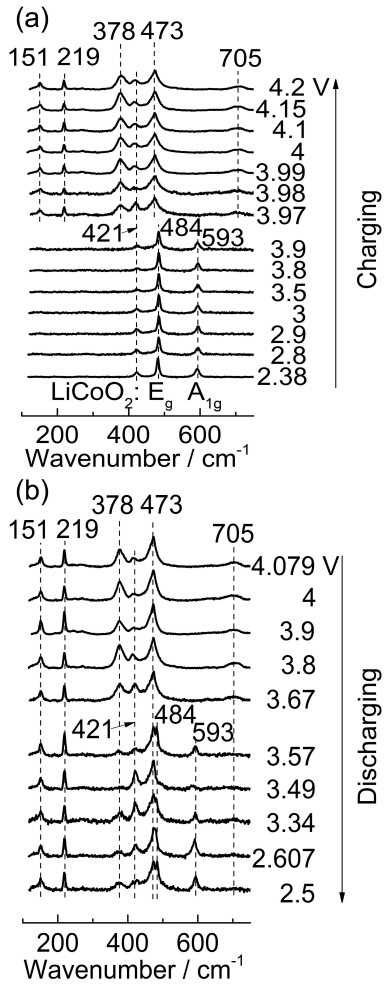

Figure 4. *In situ* Raman spectra of $LiCoO_2/Li_6PS_5Cl$ interface during a) charging to 4.2 V and b) discharging to 2.5 V.

To investigate the longer-term evolution of the $Li_6PS_5Cl/LiCoO_2$ interface a cell was run for 10 charge/discharge cycles and then characterised via *ex situ* Raman after, as shown in Figure S5. The formation of S and P_2S_x was again detected after cycling, which concurred with the in situ Raman measurement.

Both *ex situ* and *in situ* Raman analysis highlights the instability of Li_6PS_5Cl against both metallic Li or $LiCoO_2$. The formation of insulating Li_2S, S and P_2S_x at the interface lead to the increase of interfacial impedance that hampers long-term cycling of ASSBs, as widely observed in the literature. To avoid direct contact to lithium metal or positive electrode materials it is therefore necessary to look to the design of stable Li-ion conducting interlayers. These could be either polymeric or inorganic in nature and then sandwiches between the solid electrolyte and electrode active materials to prevent the formation on insulating side reaction products. Through specific cell design allowing optical access, Raman microscopy can be therefore employed to further understand the complex nature and interplay various buried interfacial regions as they evolve as a function of time, rate of charge/discharge and potential. *In situ* Raman microscopy has been shown to be a useful complimentary tool to study the interface between solid electrolytes and battery electrodes with the capability to deliver both chemical and spatial sensitive (ca. 1 μm^2) information, and this will be the focus of ongoing work.

3. Conclusions

The interface between Li_6PS_5Cl solid electrolyte with metallic Li or $LiCoO_2$ was studied with both *in situ* and *ex situ* Raman microscopy. Li_2S formation were detected during lithium deposition with Li_6PS_5Cl. Polysulfides, and P_2S_x species were detected at $Li_6PS_5Cl/LiCoO_2$ interface during charging. The *in situ* Raman results on Li_6PS_5Cl solid-state batteries demonstrate the feasibility of the *in situ* Raman cell set up, in accessing solid/solid interfaces within composite positive electrodes and lithium/solid electrolytes. This method can be translated to other solid electrolytes and present a powerful tool for the understanding the evolution interfaces within solid-state batteries under potential control.

Experimental Section

Materials preparation

Li_6PS_5Cl was synthesised by ball milling the mixture of Li_2S, P_2S_5 and LiCl, as described by J. Kasemchainan et al.[8] The materials were handled within an argon glovebox ($O_2 < 0.1$ ppm, $H_2O <$ 0.1 ppm). Stoichiometric amounts of Li_2S, P_2S_5 and LiCl powders (all from Sigma Aldrich, 99% purity) were weighed to produce a total mass of 2 g Li_6PS_5Cl. The powders were mixed by pestle and mortar for 10 minutes. The airtight zirconia jars (45 ml containing sixteen 10 mm-diameter zirconia balls) were equally filled with the mixture. The high-energy ball-milling process (Fritsch Pulverisette 7) was carried out twice, at a rotation speed of 600 rpm for 7 h. After the initial 7-h of ball-milling the jars were transferred back into the glovebox to loosen stuck powder form the jar wall. The jars were

© 2020 The Authors. Published by Wiley-VCH Verlag GmbH & Co. KGaA

25666223, 2020, 7, Downloaded from https://chemistry-europe.onlinelibrary.wiley.com/doi/10.1002/batt.201900218 by University of Ulsan, Wiley Online Library on [11/11/2025]. See the Terms and Conditions (https://onlinelibrary.wiley.com/terms-and-conditions) on Wiley Online Library for rules of use; OA articles are governed by the applicable Creative Commons License

then closed and loaded in the ball mill apparatus for further 7 h. After a total time of 14 h of ball-milling the powder was recovered and ground with pestle and mortar to remove agglomerates.

Electrochemical measurements

Cyclic voltammetry to examine the potential stability window of Li_6PS_5Cl was measured from −0.5 to 7 V vs Li^+/Li (1st cycle) and 8 V vs Li^+/Li (2nd cycle) at 30 °C in a stainless steel / Li cell within a Swagelok type cell. The scan rate was 10 mV/ s. Impedance spectroscopy was performed with a Gamry Interface-1000 device. Li foil was pressed onto the solid electrolyte pellet on both sides with a clamping pressure of 7 MPa. The voltage amplitude was 10 mV. The frequency range was from 1 MHz to 0.2 Hz. The impedance spectrum was fitted with ZView software.

Raman microscopy

Ex situ and *in situ* Raman measurements were collected using a Raman microscope (Renishaw, in via Reflex coupled with an inverted Leica microscope), with a 633 nm laser as excitation source (power < 300 μW), focussed onto the sample using a ×50 objective (Olympus). The collected Raman spectra were baseline corrected and peaks fitted using a combined Lorentzian and Gaussian function. Spectral measurement time was 2 seconds with 30 accumulations to ensure good signal to noise ratio to resolve peaks. To check for potential laser damage, Li_6PS_5Cl was measured with varying laser intensities and exposure times (Figure S6). No changes in the spectra were observed.

For the assembly of the solid-state *in situ* Raman cell, the solid electrolyte was prepared via (diameter: 5 mm) loading into a die and levelled by means of a cylindrical plunger (< 5 MPa), then the mixture of solid electrolyte, $LiCoO_2$ and carbon black (55:40:5 in weight ratio) was ground in a pestle and mortar for 30 minutes and spread uniformly onto the solid electrolyte pellet and pressed at 360 MPa for 5 minutes. 25 mg argyrodite was used as a separator layer between the positive and negative electrode for one pellet. The total amount of the cathode composite was 3.5 mg. The active material loading was 7.1 mg$LiCoO_2$/cm^2 (~1 mAh/cm^2). A polished lithium metal disk (diameter: 5 mm, Sigma Aldrich) was subsequently pressed onto the other side of the solid electrolyte and sealed in the airtight optical Raman test EL-cell (ECC-Opto-Std). All these handling was performed within an argon containing glovebox.

For the lithium stability measurements, 50 nm of Cu was deposited onto the borosilicate glass window at room temperature within the Moorfield Minilab 080 chamber and used as the current collector for lithium plating. The deposition thickness was controlled by the Inficon SQC-310 C deposition controller. For the $LiCoO_2$ stability test, 50 nm of Au was deposited onto the glass window with a transparent round area in the middle within the Univex 300 chamber. The deposition thickness was controlled by a Maxtek thickness monitor (TM-400). The diameter of the round area was 3 mm. A schematic of the in situ Raman cell set up is displayed in Figure 5. A pressure of 0.75 MPa was applied onto the solid-state battery via the spring on the back contact with the metallic lithium to ensure good contact within the solid state cell and also with the contact pin. For the *in situ* Raman measurement, a potential or current can be applied between the Au/Cu layer at room temperature via a potentiostat (Biologic). The cell was charged and discharged at a rate of 0.1 C for the $LiCoO_2$ stability study. As the $LiCoO_2$ was pressed together with the solid electrolyte, the charge and discharge capacities were calculated based on the nominal weight of the active materials for each pellet. For the *in situ* Raman measurement of the $LiCoO_2/Li_6PS_5Cl$/Li all solid state cell, the laser was focused directly onto the composite positive electrode through a 3 mm diameter transparent round area in the glass without the Au coating (similar to a holed configuration), as shown schematically in Figure 5. For the *ex situ* Raman measurement, the sample was sealed in a hermetically sealed ex situ measurement cell with an optical glass window within the glovebox.

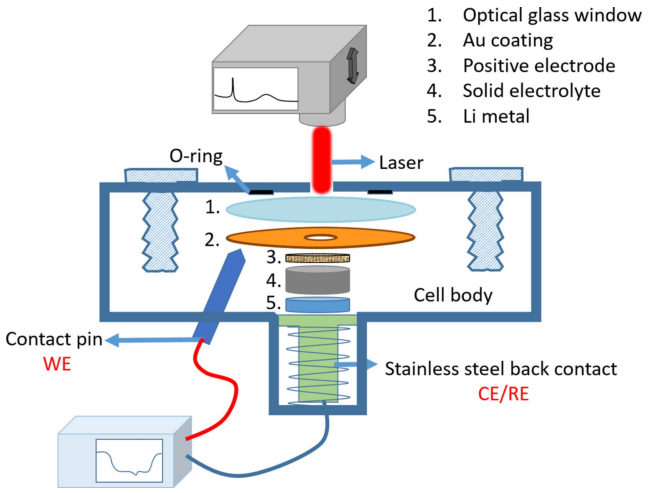

Figure 5. Schematic of the in situ Raman cell set up. WE: working electrode, CE/RE: counter electrode/reference electrode.

Acknowledgements

We gratefully acknowledge the support of ISCF Faraday Challenge project: "SOLBAT – The Solid-State (Li or Na) Metal-Anode Battery" under grant number EP/R042047/1.

Conflict of Interest

The authors declare no conflict of interest.

Keywords: electrode-solid electrolyte interface · electrochemistry · in situ Raman microscopy · interfaces · solid-state batteries

[1] J. Janek, W. G. Zeier, *Nat. Energy* **2016**, *1*, 16141.
[2] N. Kamaya, K. Homma, Y. Yamakawa, M. Hirayama, R. Kanno, M. Yonemura, T. Kamiyama, Y. Kato, S. Hama, K. Kawamoto, A. Mitsui, *Nat. Mater.* **2011**, *10*, 682–686.
[3] H. J. Deiseroth, S. T. Kong, H. Eckert, J. Vannahme, C. Reiner, T. Zaiss, M. Schlosser, *Angew. Chem. Int. Ed.* **2008**, *47*, 755–758.
[4] B. R. Shin, Y. J. Nam, D. Y. Oh, D. H. Kim, J. W. Kim, Y. S. Jung, *Electrochim. Acta* **2014**, *146*, 395–402.
[5] Y. Zhu, X. He, Y. Mo, *J. Mater. Chem. A*, **2016**, *4*, 3253–3266.
[6] J. Auvergniot, A. Cassel, J.-B. Ledeuil, V. Viallet, V. Seznec, R. Dedryvère, *Chem. Mater.* **2017**, *29*, 3883–3890.
[7] a) A. C. Luntz, J. Voss, K. Reuter, *J. Phys. Chem. Lett.* **2015**, *6*, 4599–4604; b) G. Vardar, W. J. Bowman, Q. Lu, J. Wang, R. J. Chater, A. Aguadero, R. Seibert, J. Terry, A. Hunt, I. Waluyo, D. D. Fong, A. Jarry, E. J. Crumlin, S. L. Hellstrom, Y.-M. Chiang, B. Yildiz, *Chem. Mater.* **2018**, *30*, 6259–

© 2020 The Authors. Published by Wiley-VCH Verlag GmbH & Co. KGaA

25666223, 2020, 7, Downloaded from https://chemistry-europe.onlinelibrary.wiley.com/doi/10.1002/batt.201900218 by University of Ulsan, Wiley Online Library on [11/11/2025]. See the Terms and Conditions (https://onlinelibrary.wiley.com/terms-and-conditions) on Wiley Online Library for rules of use; OA articles are governed by the applicable Creative Commons License

6276; c) Y. Xiao, Y. Wang, S.-H. Bo, J. C. Kim, L. J. Miara, G. Ceder, *Nat. Rev. Mater.* **2019**, https://doi.org/10.1038/s41578-41019-40157-41575.
[8] J. Kasemchainan, S. Zekoll, D. S. Jolly, Z. Ning, G. O. Hartley, J. Marrow, P. G. Bruce, *Nat. Mater.* **2019**, *18*, 1105–1111.
[9] N. Zhang, X. Long, Z. Wang, P. Yu, F. Han, J. Fu, G. Ren, Y. Wu, S. Zheng, W. Huang, C. Wang, H. Li, X. Liu, *ACS Appl. Energy Mater.* **2018**, *1*, 5968–5976.
[10] W. Zhang, D. A. Weber, H. Weigand, T. Arlt, I. Manke, D. Schroder, R. Koerver, T. Leichtweiss, P. Hartmann, W. G. Zeier, J. Janek, *ACS Appl. Mater. Interfaces* **2017**, *9*, 17835–17845.
[11] W. Zhang, F. H. Richter, S. P. Culver, T. Leichtweiss, J. G. Lozano, C. Dietrich, P. G. Bruce, W. G. Zeier, J. Janek, *ACS Appl. Mater. Interfaces* **2018**, *10*, 22226–22236.
[12] S. Wenzel, S. J. Sedlmaier, C. Dietrich, W. G. Zeier, J. Janek, *Solid State Ionics* **2018**, *318*, 102–112.
[13] T. Cheng, B. V. Merinov, S. Morozov, W. A. Goddard, *ACS Energy Lett.* **2017**, *2*, 1454–1459.
[14] S. H. Bo, K. W. Nam, O. J. Borkiewicz, Y. Y. Hu, X. Q. Yang, P. J. Chupas, K. W. Chapman, L. Wu, L. Zhang, F. Wang, C. P. Grey, P. G. Khalifah, *Inorg. Chem.* **2014**, *53*, 6585–6595.
[15] J. Liu, P. S. Whitfield, M. R. Saccomanno, S. H. Bo, E. Hu, X. Yu, J. Bai, C. P. Grey, X. Q. Yang, P. G. Khalifah, *Angew. Chem. Int. Ed.* **2017**, *139*, 9192–9202.
[16] Z. Wang, D. Santhanagopalan, W. Zhang, F. Wang, H. L. Xin, K. He, J. Li, N. Dudney, Y. S. Meng, *Nano Lett.* **2016**, *16*, 3760–3767.
[17] K. Yamamoto, Y. Iriyama, T. Asaka, T. Hirayama, H. Fujita, C. A. Fisher, K. Nonaka, Y. Sugita, Z. Ogumi, *Angew. Chem. Int. Ed.* **2010**, *49*, 4414–4417.
[18] a) J.-C. Panitz, P. Novák, *J. Power Sources* **2001**, *97–98*, 174–180; b) R. Baddour-Hadjean, J.-P. Pereira-Ramos, *Chem. Rev.* **2010**, *110*, 1278–1319; c) J. Lei, F. McLarnon, R. Kostecki, *J. Phys. Chem. B* **2005**, *109*, 952–957; d) P. Novák, J.-C. Panitz, F. Joho, M. Lanz, R. Imhof, M. Coluccia, *J. Power Sources* **2000**, *90*, 52–58.
[19] S. Yubuchi, S. Teragawa, K. Aso, K. Tadanaga, A. Hayashi, M. Tatsumisago, *J. Power Sources* **2015**, *293*, 941–945.
[20] L. Sang, R. T. Haasch, A. A. Gewirth, R. G. Nuzzo, *Chem. Mater.* **2017**, *29*, 3029–3037.
[21] S. Boulineau, M. Courty, J.-M. Tarascon, V. Viallet, *Solid State Ionics* **2012**, *221*, 1–5.
[22] M. Ishii, K. Shibata, H. Nozaki, *J. Solid State Chem.* **1993**, *105*, 504–511.
[23] M. Inaba, Y. Iriyama, Z. Ogumi, Y. Todzuka, A. Tasaka, *J. Raman Spectrosc.* **1997**, *28*, 613–617.
[24] a) S. N. White, *Chem. Geol.* **2009**, *259*, 240–252; b) P. Boolchand, P. Chen, U. Vempati, *J. Non-Cryst. Solids* **2009**, *355*, 1773–1785.
[25] a) Q. Pang, X. Liang, A. Shyamsunder, L. F. Nazar, *Joule* **2017**, *1*, 871–886; b) C. Dietrich, D. A. Weber, S. Culver, A. Senyshyn, S. J. Sedlmaier, S. Indris, J. Janek, W. G. Zeier, *Inorg. Chem.* **2017**, *56*, 6681–6687; c) Y. Aihara, S. Ito, R. Omoda, T. Yamada, S. Fujiki, T. Watanabe, Y. Park, S. Doo, *Front. Energy Res.* **2016**, *4*, 18(11–18); d) J. Hassoun, R. Verrelli, P. Reale, S. Panero, G. Mariotto, S. Greenbaum, B. Scrosati, *J. Power Sources* **2013**, *229*, 117–122; e) T. Rodl, R. Weihrich, J. Wack, J. Senker, A. Pfitzner, *Angew. Chem. Int. Ed.* **2011**, *50*, 10996–11000; f) Z.-L. Huang, J.-T. Zhao, J.-X. Mi, S.-Y. Mao, L.-S. Zheng, *J. Solid State Chem.* **1999**, *144*, 388–391; g) L. Koudelka, M. Pisárčik, M. S. Gutenev, L. N. Blinov, *J. Mater. Sci. Lett.* **1989**, *8*, 933–934.
[26] a) D. Himmel, L. C. Maurin, O. Gros, J. L. Mansot, *Biol. Cell* **2009**, *101*, 43–54; b) S. Bhagavantam, *Phys. Rev.* **1938**, *53*, 1015–1015.
[27] a) B. Bertheville, H. Bill, H. Hagemann, *J. Phys. Condens. Matter* **1998**, *10*, 2155–2169; b) Q. Zhao, X. Hu, K. Zhang, N. Zhang, Y. Hu, J. Chen, *Nano Lett.* **2015**, *15*, 721–726; c) T. Takeuchi, H. Kageyama, K. Nakanishi, T. Ohta, A. Sakuda, H. Sakaebe, H. Kobayashi, K. Tatsumi, Z. Ogumi, *ECS Electrochem. Lett.* **2014**, *3*, A31–A35; d) T. A. Yersak, T. Evans, J. M. Whiteley, S.-B. Son, B. Francisco, K. H. Oh, S.-H. Lee, *J. Electrochem. Soc.* **2014**, *161*, A663–A667.
[28] a) S.-Y. Wang, W. Wang, Z.-H. Lu, *Mater. Sci. Eng. B* **2003**, *103*, 184–188; b) H. S. S. Rangel, A. C. Castillo, J. F. H. Paz, J. R. F. Mancilla, H. C. Montes, P. E. G. Casillas, C. A. M. Perez, C. A. R. González, *Chalcogenide Lett.* **2015**, *12*, 381–387; c) A. Phuruangrat, T. Thongtem, S. Thongtem, *Chalcogenide Lett.* **2011**, *8*, 291–295.
[29] H. Y. Park, S. R. Lee, Y. J. Lee, B. W. Cho, W. I. Cho, *Mater. Chem. Phys.* **2005**, *93*, 70–78.

Manuscript received: December 16, 2019
Revised manuscript received: February 14, 2020
Accepted manuscript online: February 28, 2020
Version of record online: March 18, 2020

© 2020 The Authors. Published by Wiley-VCH Verlag GmbH & Co. KGaA

25666223, 2020, 7, Downloaded from https://chemistry-europe.onlinelibrary.wiley.com/doi/10.1002/batt.201900218 by University of Ulsan, Wiley Online Library on [11/11/2025]. See the Terms and Conditions (https://onlinelibrary.wiley.com/terms-and-conditions) on Wiley Online Library for rules of use; OA articles are governed by the applicable Creative Commons License